THE GEOLOGICAL SOCIETY OF AMERICA®

Seismically anisotropic magma reservoirs underlying silicic calderas

Chengxin Jiang[1], Brandon Schmandt[1], Jamie Farrell[2], Fan-Chi Lin[2], and Kevin M. Ward[2]
[1]Department of Earth and Planetary Sciences, The University of New Mexico, Albuquerque, New Mexico 87131, USA
[2]Department of Geology and Geophysics, The University of Utah, Salt Lake City, Utah 84112, USA

ABSTRACT

Seismic anisotropy can illuminate structural fabrics or layering with length scales too fine to be resolved as distinct features in most seismic tomography. Radial anisotropy, which detects differences between horizontally (V_{SH}) and vertically (V_{SV}) polarized shear wave velocities, was investigated beneath Yellowstone caldera (Wyoming, United States) and Long Valley caldera (California). Significant positive radial anisotropy indicating $V_{SH} > V_{SV}$ and low isotropic velocities, were found beneath both calderas at ~5–18 km depths. The positive radial anisotropy (>8%) volumes beneath the calderas are anomalously strong compared to the surrounding areas. The absence of a similar anisotropic signal in the wake of the propagating Yellowstone hotspot indicates that the radial anisotropy diminishes after the locus of voluminous silicic magmatism moves. We propose that the anisotropic volumes represent sill complexes of compositionally evolved magma, and the magma's seismic contrast with the crust would largely fade upon crystallization. The similarity of magma reservoir anisotropy in varied tectonic settings suggests that such mid-crustal sill complexes may be ubiquitous features of silicic caldera–forming magmatic systems, and that anisotropy should be considered to seismically estimate melt content and mobility. The absence of similar radial anisotropy in the lower crust beneath the calderas suggests lower melt fractions or a transition in the geometry of magma pathways.

INTRODUCTION

The 0.64 Ma Yellowstone caldera (Wyoming, United States) and 0.76 Ma Long Valley caldera (California) are the results of the two largest silicic volcanic eruptions since 1 Ma in the western United States; the two caldera-forming eruptions generated ~1000 and 600 km^3 of dense rock equivalent pyroclastic materials, respectively (Christiansen 2001; Hildreth and Wilson, 2007). The eruptibility and hazard of volcanic systems primarily depends on the melt fraction and distribution within magma reservoirs (e.g., Lowenstern et al., 2017). Therefore, better understanding the architecture of existing crustal magma reservoirs is valuable for estimating the impact of potential eruptions and developing effective models of voluminous silicic magmatic systems.

Seismic tomography of the crust beneath areas of silicic caldera-forming eruptions reveals that low-velocity zones at ~5–20 km depth are common, and these are usually interpreted as shallow reservoirs of evolved magma (e.g., Huang et al., 2015; Seccia et al., 2011). While the location and geometry of magmatic low-velocity bodies are frequently constrained by tomographic inversions, less is known about the configuration of melts within reservoirs or pathways connecting reservoirs. Geochemical studies suggest that magma reservoirs grow through variable rates of incremental accumulation of sills and dikes, whose melt contents may not be well-mixed across the composite reservoir (Cashman and Giordano, 2014).

At Yellowstone, spatially variable expansion and subsidence of magmatic sills at ~7–10 km depth is suggested to drive temporal variations in surface deformation (Chang et al., 2010). In contrast, geodetic records at Long Valley caldera over the past few decades have been dominated by nearly monotonic but temporally variable uplift rates, with an estimated source of inflation at ~7 km depth (Montgomery-Brown et al., 2015). The inferred depths of the inflation sources at both volcanoes are approximately coincident with the tops of seismically inferred shallow magma reservoirs (Seccia et al., 2011; Huang et al., 2015).

A recent seismic study at the Toba caldera (Indonesia) identified an anisotropic signature that was interpreted to represent a magmatic sill complex spanning most of the crustal column (Jaxybulatov et al., 2014); this was suggested to support models of long-term incremental evolution of magma bodies through successive intrusions of sills (e.g., Annen et al., 2006). However, it is unclear if that anisotropic signal extends through the entire crustal column, or if it is a common feature of other silicic caldera–forming magmatic systems. Here we report seismic evidence for strong anisotropy at remarkably similar depths beneath Yellowstone and Long Valley calderas.

DATA AND METHODS

Continuous seismic data were compiled from previous larger-scale studies (Schmandt et al., 2015; Jiang et al., 2018) and augmented by local networks (Fig. 1; Table DR1 in the GSA Data Repository[1]). Ambient noise interferometry was performed following the methods of Bensen et al. (2007) to estimate inter-station empirical Green's functions, and phase velocities of Rayleigh and Love waves at 3–30 s and 5–30 s for Long Valley, and 6–25 s for Yellowstone. Slight differences in the period ranges result from the requirement of surface wave signal-to-noise ratios of >6. The inter-station phase velocity measurements were inverted for two-dimensional (2-D) phase velocity maps (Fig. DR3) using a fast-marching–based ray tracing method (Rawlinson and Sambridge, 2003), and uncertainties were estimated using repeated inversions with bootstrap resampling of the data. A Bayesian Markov Chain Monte Carlo (MCMC) inversion scheme (Shen et al., 2012) was applied to jointly invert Rayleigh and Love wave dispersion data.

The inversion for shear velocities was carried out in two steps. First, the local Rayleigh and Love wave dispersion curves were fit with an isotropic model ($V_{SV} = V_{SH}$, V_{SH}—horizontally polarized shear wave velocity, and V_{SV}—vertically polarized). Large misfits from the isotropic inversion (Figs. DR5 and DR6) indicate the likely presence of radial anisotropy (e.g., Jaxybulatov et al., 2014). A second inversion was conducted in which V_{SV} and V_{SH} were allowed to vary independently. During the anisotropic inversion, V_{SV} and V_{SH} were evaluated simultaneously and the amplitude of radial anisotropy is defined as $100\%*(V_{SH}-V_{SV})/(V_S)$, where V_S is the Voigt average of V_{SH} and V_{SV}. The values of

[1]GSA Data Repository item 2018264, details on data sources, analysis methods, and synthetic tests, including Figures DR1–DR10, and Tables DR1 and DR2, is available online at http://www.geosociety.org/datarepository/2018/, or on request from editing@geosociety.org. The raw seismic data from this study are publicly available via the IRIS DMC (Incorporated Research Institutions for Seismology Data Management Center, http://ds.iris.edu/ds/nodes/dmc/).

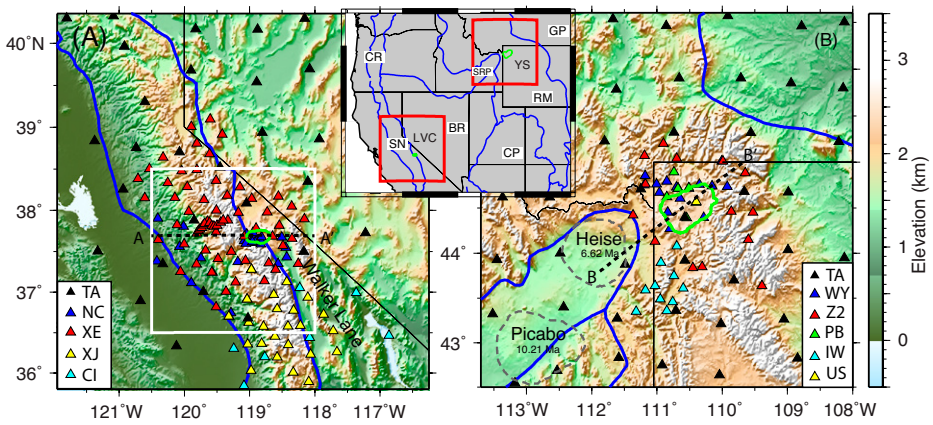

Figure 1. Study area maps, showing Long Valley, California (A) and Yellowstone, Wyoming (B) regions. LVC—Long Valley caldera; YS—Yellowstone caldera. Physiographic provinces are outlined in blue, and labeled in the inset map, including Sierra Nevada (SN), Cascade Range (CR), Basin and Range (BR), Snake River Plain (SRP), Colorado Plateau (CP), Rocky Mountain (RM) and Great Plains (GP). Thin black lines are the state borders, and thick green lines delineate the calderas. Triangles represent seismic stations: black represents Transportable Array (TA) stations and other colors denote regional networks or temporary arrays (see Table DR1 [see footnote 1] for seismic network information). White box in A is the area shown in Figure 2. Dashed gray lines in B denote the Heise and Picabo calderas. A-A′ and B-B′ show locations of transects shown in Figure 3.

V_{SV} and V_{SH} in the Monte Carlo search were constrained within the bounds shown in Table DR2. The posterior distribution was defined as the 800 best-fitting models after 1.5 million MCMC iterations, and we ensured that the distributions were not biased by the search bounds. The number of iterations was chosen to achieve a stable mean and 95% uncertainty for the posterior distributions. To estimate where radial anisotropy is required to fit the dispersion data, we plotted the areas where zero anisotropy is located outside of the 95% confidence zone (Fig. 2). Radial anisotropy images with varying uncertainty thresholds are shown in Figures DR7 and DR8.

ISOTROPIC AND ANISOTROPIC RESULTS

The isotropic and anisotropic results exhibit contrasting regional settings and similar local characteristics beneath the two calderas (Fig. 2).

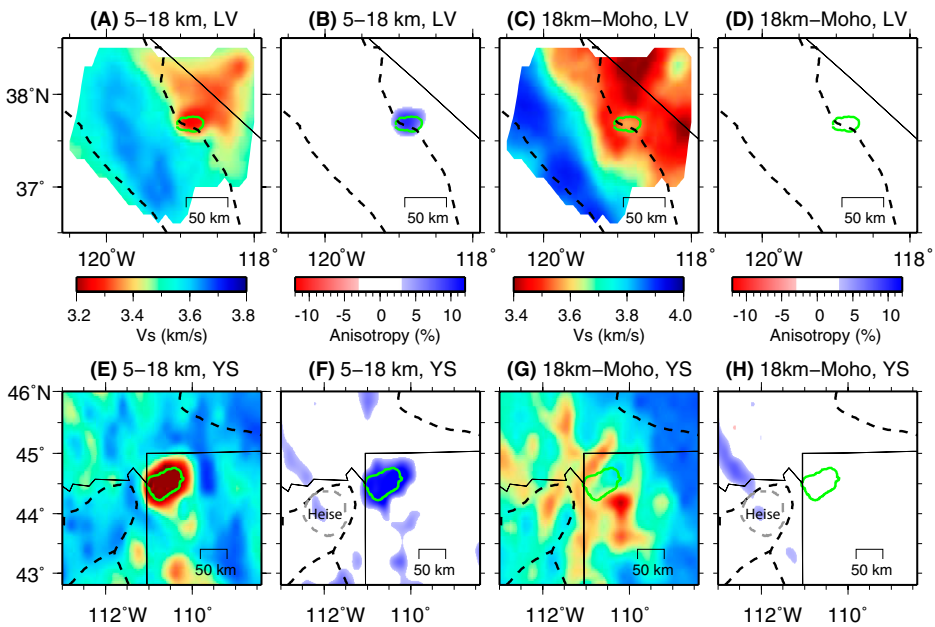

Figure 2. Isotropic shear wave velocity (Vs) and anisotropic maps averaged at different depth ranges. LV—Long Valley caldera, California, USA; YS—Yellowstone caldera, Wyoming. Black dashed lines represent physiographic provinces, and thick green lines delineate the calderas. Gray dashed lines in F and H show the Heise caldera. The same Vs color scale is used for both study areas, but spatial scale of the maps differs, as shown by the 50 km scale bars.

The contrasting upper crustal structures at <5 km depth (Fig. DR10) are not a focus here, as we are primarily concerned with deeper crustal structure. Long Valley caldera sits along a dramatic crustal boundary, with much slower crustal velocities in the Walker Lane to the east than the Sierra Nevada batholith to the west. The crust surrounding Yellowstone caldera generally has higher velocities than the Walker Lane east of Long Valley caldera. Both velocity models include regionally anomalous low velocities at ~5–18 km depth (Figs. 2A and 2E). The middle-to-upper crustal low-velocity anomaly beneath Yellowstone spans a larger area compared to the velocity anomaly beneath Long Valley, similar to the differences in the areas of the overlying calderas. The most striking feature in the middle-to-upper crust is the coincidence of the concentrated low isotropic velocities with strong positive radial anisotropy beneath the calderas. The average strength of radial anisotropy from 5 to 18 km is 8% at Long Valley and 12% at Yellowstone. In both study areas, the strongest radial anisotropy is located at 5–18 km beneath the calderas.

Tomography images of the lower crust show less-dramatic isotropic velocity variations and a relative scarcity of significant radial anisotropy in both calderas (Fig. 2). Lower-crustal velocities beneath both calderas are slightly higher than in the surrounding regions, but both areas have low-velocity anomalies that are slightly offset from the caldera locations. At Long Valley, the low-velocity anomaly at ~20 km depth is offset to the west beneath Mammoth Mountain, near the location where deep crustal seismicity has been observed (Shelly and Hill, 2011). At Yellowstone, the lower-crustal low velocities are offset just south and west of the caldera, which is different from a recent P-wave tomography image that showed low velocities in the lower crust beneath the caldera, albeit with the lowest velocities beneath the southwestern end of the caldera (Huang et al., 2015). Radial anisotropy is markedly different in the lower crust compared to the middle-to-upper crust, as it is not required at depths between 18 km and the local Moho (Fig. 2; Figs. DR7 and DR8). Synthetic tests demonstrate that the inversion scheme can distinguish between positive anisotropy confined to 5–18 km depth and anisotropy extending to the Moho (Fig. DR9).

MIDDLE-TO-UPPER CRUSTAL MAGMATIC SILL COMPLEXES

Strong positive radial anisotropy at ~5–18 km depth beneath both calderas indicates horizontal layering of heterogeneous materials (Fig. 3), which we interpret as magmatic sill complexes similar to that beneath the Toba caldera (Jaxybulatov et al., 2014). Sub-solidus sills of an anomalous lithology could also produce radial anisotropy (Backus, 1962). Given that isotropic

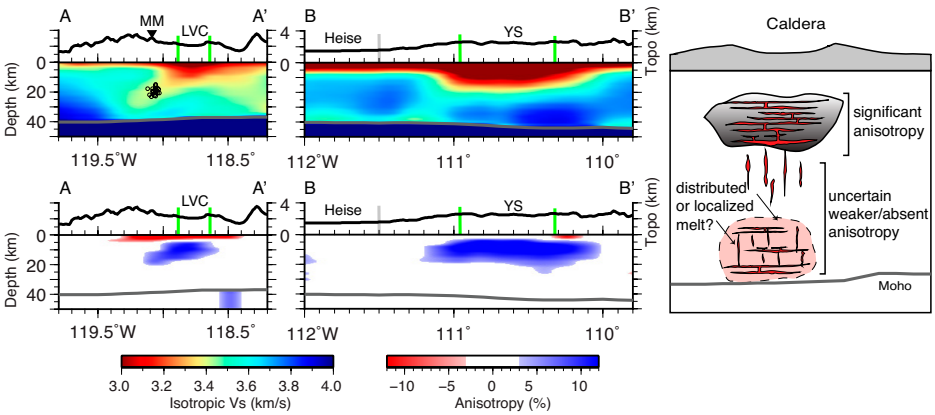

Figure 3. Vertical cross sections of isotropic shear wave velocity (Vs) and anisotropy. Long Valley caldera (LVC), California, USA (A-A′) and Yellowstone caldera (YS), Wyoming (B-B′), and an interpretative cartoon. Profile locations are marked in Figure 1. Horizontal gray lines illustrate the Moho. Vertical green lines delineate the calderas. Circles in the first cross section of LVC are hypocenters from a 2009 earthquake swarm (Shelly and Hill et al., 2011). Note that the depths in the tomography are relative to the local surface, and the cartoon figure is shown with a different scale.

Vs in the positive radial anisotropy volumes is lower than in the surrounding crust (Fig. 2), and that further Vs reduction is needed in the sills to achieve the ~10% anisotropy beneath the calderas, we consider a partial melt origin more likely. The eastern Snake River Plain provides a time-dependent view of the anisotropic structure underlying the Yellowstone hotspot that is consistent with a melt origin. The Heise caldera complex (Fig. 1B), which was active from ca. 6.6 to 4.5 Ma (Watts et al., 2011), is not underlain by a similar volume of significant positive radial anisotropy nor isotropic low velocities at ~5–18 km depth. This suggests that the radially anisotropic structure imaged beneath Yellowstone caldera is a transient feature that would fade if the hotspot's locus of silicic magmatism migrates. For the anisotropy to fade, most of the partial melt within the sills must have compositionally evolved from the primitive basalts supplied by mantle melting, to more felsic compositions typical of the continental crust.

The presence of a magmatic sill complex at similar depth ranges beneath Toba (Jaxybulatov et al., 2014), Yellowstone, and Long Valley calderas provides important evidence for common properties of voluminous silicic magmatic systems in diverse tectonic settings. Construction of the evolved magma reservoir as a sill complex is consistent with conceptual models of incrementally assembled and heterogeneous magma reservoirs, rather than a single well-mixed melt body (Cashman and Giordano, 2014). Melt storage in weakly connected volumes like sills also agrees with geochemical variability of magmas erupted from individual calderas (Gualda and Ghiorso, 2013; Swallow et al., 2018). Crystal mushes in sill complexes could be the long-lived staging grounds for eruptions that are eventually sourced by shorter-term accumulation of eruptible melts in the uppermost ~5–8 km, as suggested by geodynamic models (Gelman et al., 2013) and petrologic constraints (Gualda and Ghiorso, 2013). Indeed, recent geochemical evidence favors long-lived (10^4–10^5 yr) crystal-rich magma reservoirs that rapidly mobilize due to high flux recharge events within ~10^{-1} to 10^3 yr of eruption (Till et al., 2015; Rubin et al., 2017).

IMPLICATIONS FOR EVALUATING MAGMA RESERVOIRS

When estimating the current life-cycle stage and hazards of active magmatic systems, the total melt content and melt mobility are key properties. Our new results caution that seismic estimates of those properties at large silicic magmatic systems could be biased by anisotropy. Reductions of V_{SV} sampled by Rayleigh waves (e.g., Stachnik et al., 2008) and P-to-S_V conversions (e.g., Chu et al., 2010) are often used to estimate the average melt fraction in magma reservoirs. Introduction of ~10% positive radial anisotropy could bias Vs estimates by up to ~0.15 km/s for typical crustal velocities. The actual bias may be smaller depending on the sill's velocity anomaly and thickness (Jaxybulatov et al., 2014). For reference, a 0.15 km/s bias toward lower velocities would overestimate melt fractions by ~4% for low melt fractions (< 20%) using the rhyolitic melt to Vs relationship from Chu et al. (2010), which is specific to Yellowstone rhyolite composition. At higher melt fractions, the potential bias would increase. The mean isotropic Vs values from 5 to 18 km beneath Long Valley and Yellowstone calderas correspond to volumetrically averaged rhyolitic melt fraction estimates of 1.5% and 6%, respectively, which would increase to 4% and 10% if only V_{SV} were considered. Such estimation is still within the range of 5%–32% melts estimated by previous studies for Yellowstone (Chu et al., 2010; Huang et al., 2015). We may underestimate the melt fraction present in subset volumes of the two anomalies because the horizontal-resolution length scale of our tomography is ~22 km for Long Valley and ~33 km for Yellowstone (Fig. DR2).

Even if seismic anisotropy is considered, the concentration of partial melts in sills that are inter-layered with more crystal-rich layers (e.g., Ellis et al., 2014) can introduce another type of bias. Melt fractions estimated by seismically averaging the entire volume of the sill complex (including more crystal-rich layers) will underestimate the melt fraction within individual sills, and hence overestimate the partial melt's viscosity (Costa et al., 2009). This difference is important with respect to the stability of magmatic systems because weakly connected, but relatively high melt-fraction sills could more rapidly mobilize their melts into eruptible reservoirs (e.g., Cashman and Giordano, 2014), which may not be expected based on the volumetrically averaged properties of the magmatic system. Future studies using numerical modeling of wave propagation or active source experiments to investigate fine sill structures could provide valuable new insights.

CHANGES IN THE MAGMATIC SYSTEMS WITH DEPTH

The radially anisotropic inversions show that anisotropy is required at 95% confidence in the middle-to-upper crust, but none of the Long Valley study area, and only a small fraction near the western edge of the Yellowstone study area, require radial anisotropy in the lower crust at 95% confidence. The areas of radial anisotropy expand with less-stringent uncertainty thresholds (Figs. DR7 and DR8), but even without any culling, no radial anisotropy is found in the lower crust beneath either caldera. As demonstrated in the synthetic tests (Fig. DR9), the inversion scheme could resolve similar strength (10%) anisotropy extending from 18 km to the Moho, but it could not resolve ≤2.5% anisotropy. So, it is clear that the magnitude of anisotropy decreases in the lower crust, but it may not be strictly isotropic. The sharp decrease in the strength and significance of radial anisotropy below ~15–20 km suggests a change in the abundance and/or average geometry of melt-bearing volumes compared to the inferred sill complexes in the middle-to-upper crust (Fig. 3). Three potential scenarios are considered:

(1) If the lower-crustal melt fraction is lower, then the anisotropy may be too weak to detect even if melt is organized in sills. The average melt fraction versus depth is difficult to constrain, but prior P-wave tomography at Yellowstone was used to interpret an ~4× decrease in melt fraction in the lower crustal reservoir (Huang et al., 2015). Thus, it is plausible that less-abundant lower-crustal melt is also stored in sills.

(2) Weak or absent radial anisotropy could result from spatial averaging of sills that promote positive anisotropy (Jaxybulatov et al., 2014) and dikes that promote negative anisotropy (Mordret et al., 2015; Fig. 3).

(3) The lower crust may host partial melt that is more uniformly distributed and transported through interconnected pore spaces, rather than concentrated in melt-rich sills or dikes.

Following Huang et al. (2015), our interpretive cartoon suggests a lower-crustal reservoir of more primitive melt and a middle-to-upper crustal reservoir of felsic melt, but only the shallower anisotropic reservoir is specifically indicated by the results of this study (Fig. 3).

CONCLUSIONS

We performed radially anisotropic surface-wave tomography of the Long Valley and Yellowstone magmatic systems and found that they contain low isotropic Vs and positive radial anisotropy in similar depth ranges of ~5–18 km. The implied stratification of seismic properties, the lower-than-regional-average isotropic Vs, and the absence of both features beneath the previous location of silicic magmatism due to the Yellowstone hotspot, are all consistent with sill complexes containing compositionally evolved melts. Similar attributes in contrasting tectonic settings suggest that sill complexes are common, and perhaps ubiquitous, features of silicic caldera–forming magmatic systems. Diminished radial anisotropy below 15–20 km suggests that more-primitive lower-crustal melts are less abundant or not so strongly concentrated in sill complexes.

ACKNOWLEDGMENTS

K. Cashman, N. Shapiro, O. Bachmann, N. Harmon, and an anonymous reviewer provided helpful feedback. The study was supported by National Science Foundation grant EAR 1554908 (to Schmandt), grant CyberSEES-1442665 (to Lin), and the King Abdullah University of Science and Technology (Saudi Arabia) under award OCRF-2014-CRG3–2300 (to Lin).

REFERENCES CITED

Annen, C., Blundy, J.D., and Sparks, R.S.J., 2006, The genesis of intermediate and silicic magmas in deep crustal hot zones: Journal of Petrology, v. 47, p. 505–539, https://doi.org/10.1093/petrology/egi084.

Backus, G.E., 1962, Long-wave elastic anisotropy produced by horizontal layering: Journal of Geophysical Research: Solid Earth, v. 67, p. 4427–4440, https://doi.org/10.1029/JZ067i011p04427.

Bensen, G.D., Ritzwoller, M.H., Barmin, M.P., Levshin, A.L., Lin, F., Moschetti, M.P., Shapiro, N.M., and Yang, Y., 2007, Processing seismic ambient noise data to obtain reliable broad-band surface wave dispersion measurements: Geophysical Journal International, v. 169, p. 1239–1260, https://doi.org/10.1111/j.1365-246X.2007.03374.x.

Cashman, K.V., and Giordano, G., 2014, Calderas and magma reservoirs: Journal of Volcanology and Geothermal Research, v. 288, p. 28–45, https://doi.org/10.1016/j.jvolgeores.2014.09.007.

Chang, W.L., Smith, R.B., Farrell, J., and Puskas, C.M., 2010, An extraordinary episode of Yellowstone caldera uplift, 2004–2010, from GPS and InSAR observations: Geophysical Research Letters, v. 37, https://doi.org/10.1029/2010GL045451.

Christiansen, R.L., 2001, The Quaternary and pliocene Yellowstone plateau volcanic field of Wyoming, Idaho, and Montana: U.S. Geological Survey Professional Paper 729-G, 156 p., 3 plates.

Chu, R., Helmberger, D.V., Sun, D., Jackson, J.M., and Zhu, L., 2010, Mushy magma beneath Yellowstone: Geophysical Research Letters, v. 37, https://doi.org/10.1029/2009GL041656.

Costa, A., Caricchi, L., and Bagdassarov, N., 2009, A model for the rheology of particle-bearing suspensions and partially molten rocks: Geochemistry Geophysics Geosystems, v. 10, https://doi.org/10.1029/2008GC002138.

Ellis, B.S., Bachmann, O. and Wolff, J.A., 2014, Cumulate fragments in silicic ignimbrites: The case of the Snake River Plain: Geology, v. 42, p.431-434, https://doi.org/10.1130/G35399.1.

Gelman, S.E., Gutiérrez, F.J., and Bachmann, O., 2013, On the longevity of large upper crustal silicic magma reservoirs: Geology, v. 41, p. 759–762, https://doi.org/10.1130/G34241.1.

Gualda, G.A., and Ghiorso, M.S., 2013, The Bishop Tuff giant magma body: An alternative to the Standard Model: Contributions to Mineralogy and Petrology, v. 166, p. 755–775, https://doi.org/10.1007/s00410-013-0901-6.

Hildreth, W., and Wilson, C.J.N., 2007, Compositional zoning of the Bishop Tuff: Journal of Petrology, v. 48, p. 951–999, https://doi.org/10.1093/petrology/egm007.

Huang, H.H., Lin, F.C., Schmandt, B., Farrell, J., Smith, R.B., and Tsai, V.C., 2015, The Yellowstone magmatic system from the antle plume to the upper crust: Science, v. 348, p. 773–776, https://doi.org/10.1126/science.aaa5648.

Jaxybulatov, K., Shapiro, N.M., Koulakov, I., Mordret, A., Landès, M., and Sens-Schönfelder, C., 2014, A large magmatic sill complex beneath the Toba caldera: Science, v. 346, p. 617–619, https://doi.org/10.1126/science.1258582.

Jiang, C., Schmandt, B., Hansen, S.M., Dougherty, S.L., Clayton, R.W., Farrell, J., and Lin, F.C., 2018, Rayleigh and S wave tomography constraints on subduction termination and lithospheric foundering in central California: Earth and Planetary Science Letters, v. 488, p. 14–26, https://doi.org/10.1016/j.epsl.2018.02.009.

Lowenstern, J.B., Sisson, T.W., and Hurwitz, S., 2017, Probing Magma Reservoirs to Improve Volcano Forecasts: Eos (Washington, D.C.), v. 98, https://doi.org/10.1029/2017EO085189.

Montgomery-Brown, E.K., Wicks, C.W., Cervelli, P.F., Langbein, J.O., Svarc, J.L., Shelly, D.R., Hill, D.P., and Lisowski, M., 2015, Renewed inflation of Long Valley Caldera, California (2011 to 2014): Geophysical Research Letters, v. 42, p. 5250–5257, https://doi.org/10.1002/2015GL064338.

Mordret, A., Rivet, D., Landès, M., and Shapiro, N.M., 2015, Three-dimensional shear velocity anisotropic model of Piton de la Fournaise Volcano (La Réunion Island) from ambient seismic noise: Journal of Geophysical Research: Solid Earth, v. 120, p. 406–427, https://doi.org/10.1002/2014JB011654.

Rawlinson, N., and Sambridge, M., 2003, Seismic traveltime tomography of the crust and lithosphere: Advances in Geophysics, v. 46, p. 81–198, https://doi.org/10.1016/S0065-2687(03)46002-0.

Rubin, A.E., Cooper, K.M., Till, C.B., Kent, A.J., Costa, F., Bose, M., Gravley, D., Deering, C., and Cole, J., 2017, Rapid cooling and cold storage in a silicic magma reservoir recorded in individual crystals: Science, v. 356, p. 1154–1156, https://doi.org/10.1126/science.aam8720.

Schmandt, B., Lin, F.C., and Karlstrom, K.E., 2015, Distinct crustal isostasy trends east and west of the Rocky Mountain Front: Geophysical Research Letters, v. 42, https://doi.org/10.1002/2015GL066593.

Seccia, D., Chiarabba, C., De Gori, P., Bianchi, I., and Hill, D.P., 2011, Evidence for the contemporary magmatic system beneath Long Valley Caldera from local earthquake tomography and receiver function analysis: Journal of Geophysical Research: Solid Earth, v. 116, https://doi.org/10.1029/2011JB008471.

Shelly, D.R., and Hill, D.P., 2011, Migrating swarms of brittle-failure earthquakes in the lower crust beneath Mammoth Mountain, California: Geophysical Research Letters, v. 38, https://doi.org/10.1029/2011GL049336.

Shen, W., Ritzwoller, M.H., Schulte-Pelkum, V., and Lin, F.C., 2012, Joint inversion of surface wave dispersion and receiver functions: A Bayesian Monte-Carlo approach: Geophysical Journal International, v. 192, p. 807–836, https://doi.org/10.1093/gji/ggs050.

Stachnik, J.C., Dueker, K., Schutt, D.L., and Yuan, H., 2008, Imaging Yellowstone plume-lithosphere interactions from inversion of ballistic and diffusive Rayleigh wave dispersion and crustal thickness data: Geochemistry Geophysics Geosystems, v. 9, https://doi.org/10.1029/2008GC001992.

Swallow, E.J., Wilson, C.J., Myers, M.L., Wallace, P.J., Collins, K.S. and Smith, E.G., 2018, Evacuation of multiple magma bodies and the onset of caldera collapse in a supereruption, captured in glass and mineral compositions: Contributions to Mineralogy and Petrology, v. 173, p. 33, https://doi.org/10.1007/s00410-018-1459-0.

Till, C.B., Vazquez, J.A., and Boyce, J.W., 2015, Months between rejuvenation and volcanic eruption at Yellowstone caldera, Wyoming: Geology, v. 43, p. 695–698, https://doi.org/10.1130/G36862.1.

Watts, K.E., Bindeman, I.N., and Schmitt, A.K., 2011, Large-volume rhyolite genesis in caldera complexes of the Snake River Plain: Insights from the Kilgore Tuff of the Heise Volcanic Field, Idaho, with comparison to Yellowstone and Bruneau–Jarbidge rhyolites: Journal of Petrology, v. 52, p. 857–890, https://doi.org/10.1093/petrology/egr005.

Manuscript received 15 March 2018
Revised manuscript received 2 May 2018
Manuscript accepted 30 June 2018

Printed in USA